Available online at www.sciencedirect.com

ScienceDirect

Procedia IUTAM 14 (2015) 364 – 373

Procedia IUTAM

www.elsevier.com/locate/procedia

IUTAM_ABCM Symposium on Laminar Turbulent Transition

The Combined Effects of Wavepacket Frequency, Amplitude and Bandwidth on its Transition Process in a Boundary Layer

Kean-Lee Kang[a], K.S. Yeo[b,*]

[a]*NUS Graduate School for Integrative Sciences and Engineering, National University of Singapore, Singapore 117456*
[b]*Department of Mechanical Engineering, National University of Singapore, Singapore 117576*

Abstract

Direct numerical simulations (DNS) were used to investigate the effect of frequency bandwidth on the laminar-turbulent transition of wavepackets evolving in a Blasius boundary layer under a total of 18 different combinations of wavepacket frequency, amplitude and bandwidth. Extensive comparisons with linear stability theory (LST) were also performed with a program written to automatically calculate the spatial amplification of an ensemble of modes in a wavepacket, enabling the linear and nonlinear aspects of the wavepacket development to be clearly distinguished. Input disturbances that are wide in terms of frequency bandwidth encouraged N-type (Novosibirsk) transition, while narrow-bandwidth disturbances favoured K-type (Klebanoff) transition. However, the initial amplitude and frequency composition of the wavepacket also play an important role in the transition process, with higher-amplitude initial disturbances leading to an increased number of K-type transition events, while frequency compositions that are dominated by linearly damped or slow-growing modes are more likely to transition via the N-route. Moreover, there is a certain preferred frequency of the wavepacket, corresponding to the lower branch point on the neutral stability curve at the disturbance source. The transition process appeared to be most sensitive to changes in bandwidth when the wavepacket is dominated by its preferred frequency.

Selection and peer-review under responsibility of ABCM (Brazilian Society of Mechanical Sciences and Engineering)

Keywords: laminar turbulent transition, wavepacket, boundary layer, frequency, bandwidth, amplitude

1. Introduction

1.1. Background

A Blasius boundary layer is known to transition to turbulence through several mechanisms. This work focuses on the transition via two paths, known as the K (Klebanoff) and N (Novosibirsk) regimes, as classified by Boiko et al..[1] Both regimes begin with small-amplitude disturbances in the boundary layer, that grow and develop into Λ-structures. In the K-regime, these Λ-structures are aligned with each other in the streamwise direction, and propagate downstream one after the other, along fixed lines. The aligned configuration of these structures allows them to connect to each

* Corresponding author. Tel.: +65-65162246. ; fax: +65-67791459
E-mail address: mpeyeoks@nus.edu.sg

Selection and peer-review under responsibility of ABCM (Brazilian Society of Mechanical Sciences and Engineering)
doi:10.1016/j.piutam.2015.03.061

other, giving rise to long vortical streaks known as Klebanoff modes.[2] N-regime transitions have these Λ-structures in a staggered configuration, where each row of structures appears to be offset in the spanwise direction from the rows in front of and behind it, and have been investigated thoroughly.[3] N-transition is also found in the work of Herbert,[4] hence N-type transition is also known as H-type in some publications.

The focus of this present investigation is to shed more light on when a flow might transition via the K-regime, and when it would prefer the N-regime. For individual waves of well-defined frequency, wavenumber and amplitude, much is already known about its transition route. For example, it is known that higher-amplitude waves are more likely to transition via the K-route.[1] Systems of three waves interacting with each other are also well-researched.[5,6] The challenge now is perhaps to integrate these results into a more robust framework that is better able to predict transition under the vagaries and complexities of real-world conditions.

To that end, wavepackets have presented a fruitful area of investigation.[7,8,9] Such flow disturbances are characterized by their limited spatial extent, which causes them to occupy a large Fourier space by the same mathematical mechanism as the uncertainty principle in quantum mechanics.[10] Occupying a large Fourier space implies that the wavepackets consist of a continuum of modes, of different frequency and wavenumber. This observation leads us to explore the feasibility of using an additional parameter to characterize the frequency distribution of the wavepacket- the bandwidth.

Inspiration for the use of bandwidth came from the theoretical analysis of Craik,[11] which in turn was meant to explain the experimental results of Medeiros and Gaster.[12,13] Their experiments showed that if a boundary layer flow were perturbed with a small wavepacket, whose dominant component is a two-dimensional (2D) fundamental (Tollmien-Schlichting, TS) wave, an oblique (3D) wave at about half the frequency of the fundamental would develop. This wave is known as the subharmonic, and its strength is a key spectral signature of impending N-regime transition. Craik[11] proposed a model in which the formation of the subharmonic mode requires the initial wavepacket to have a sufficiently broad bandwidth such that its frequency range is greater than or equal to the subharmonic frequency, and its range of wavenumbers is as great as the wavenumber of the subharmonic mode. In other words, wide bandwidth wavepackets are needed for N-type transition. The predictions of this theoretical analysis were supported by subsequent experiments.[14,15] Indeed, it was found that wide bandwidth wavepackets experienced rapid subharmonic mode growth, and laminar-turbulent transition via the N-regime. However, if a narrow bandwidth wavepacket were used, transition was observed to take the K-regime, with the formation of streaky structures reminiscent of Klebanoff modes.[16]

1.2. Contributions of the present study

The DNS simulations investigated 18 combinations of wavepacket frequency, amplitude and bandwidth, to elucidate the complex interplay among these factors that determines the transition path of the wavepacket. Most of the wavepackets break down to incipient turbulence within the domain, and this enabled us to have a fuller understanding of the laminar-turbulent transition process. Besides good qualitative agreement with the experimental results of Medeiros[14] and theoretical predictions of Craik,[11] the basic setup of this work was designed to closely mimic the experimental setup of Cohen's 1991 paper,[9] and good quantitative agreement was achieved, as previously reported.[17] We then built on this foundation by making changes to the amplitude, frequency and bandwidth of the initial disturbance to perform our subsequent investigations.

Moreover, our investigations leverage the ease of data collection from simulations to create graphics that clearly track the spatial development of the entire continuum of modes found in the wavepacket. Linear stability theory (LST) was also applied to predict the downstream evolution of the wavepacket. This was achieved by representing the wavepacket as an ensemble of modes of different frequency and wavenumber. The spatial amplification of each mode is calculated using classical methods[18] and the results are compared with DNS to build a picture of the overall wavepackets' development, in which the linear and nonlinear phenomena are clearly distinguished from each other. Excellent agreement between LST and DNS is found for the early stages of the wavepacket development. Of course, the agreement diminishes at later stages which are dominated by nonlinear phenomena.

One significant common result from the LST and DNS computations was the existence of a preferred wavepacket frequency. Wavepackets that were initially dominated by modes of higher frequencies displayed a tendency to shift their dominant frequency towards the preferred frequency, which corresponds to the frequency of the lower branch of

the neutral stability curve at the disturbance source. This preference was only overridden by increasing the amplitude of the dominant frequency, or decreasing the wavepacket bandwidth.

Several interesting observations also surfaced during the course of these simulations. For instance, the use of a logarithmic scale in plotting spectral data allowed features to come to light across many orders of magnitude. We attempt to explain some of these new findings by broadening our considerations beyond the traditional low-order terms in nonlinear analysis to consider the wider system of higher-order modes, such as the higher harmonics of the primary spectrum. Doing so enables a more complete picture of wavepacket evolution to come into focus.

2. Methodology

2.1. DNS simulation parameters

The direct numerical simulations (DNS) were performed using a spatial DNS code,[17,19] which involves second-order finite volume spatial discretization, and second-order backward Euler temporal discretization of the perturbation Navier-Stokes equation. The base flow is a Blasius boundary layer, and a multigrid procedure was used to deal with the pressure. More details regarding the simulation can be found in the references.[16]

The streamwise, wall-normal and spanwise coordinates are X, Y and Z respectively, and the perturbation velocities in each direction are u, v and w. Lengths are non-dimensionalized based on the reference length $\delta_{ref} = 2.3182\times10^{-3}$ m, which is the displacement thickness at the location of the disturbance source, while velocities are based on freestream velocity $U_\infty = 6.65$ m/s. The computational domain is $310 \le X \le 1510$, $0 \le Y \le 54$, $-173 \le Z \le 173$ and the mesh has grid points $1170\times65\times163$, with uniform meshing in the X and Z direction, and a stretched grid in the Y direction to increase the grid resolution close to the wall. Kinematic viscosity is $\nu = 1.49\times10^{-3}$ m^2/s. The initial disturbance is introduced into the flow by specifying the wall-normal component of the perturbation velocity, v at a single grid point at the wall, along the centerline $Z = 0$ at $X = 349$ from the leading edge with a Reynolds number $\mathrm{Re} = \delta U_\infty/u$ of 1036. Time is non-dimensionalized using $T = tU_\infty/\delta_0$, where t is in seconds.

2.2. Wavepacket production

In initial work, the frequency of the disturbance source was fixed, and the excitation duration was varied in order to generate wavepackets of different frequency bandwidth. This resulted in wavepackets with not only different bandwidth $\Delta\omega$, but also slightly different peak spectral densities ω_{max}, due to the effects of truncating an infinite-length sine wave into disturbance signals of different (finite) lengths.

Currently, this wavepacket generation mechanism has been refined to maintain a constant peak spectral density in each wavepacket, even though each wavepacket has a different bandwidth. This is achieved by altering the disturbance source frequency ω_0 to compensate for the effects of finite-duration signals. In other words, ω_0 is varied so that ω_{max} remains constant even though the bandwidth changes. The disturbance duration T_d is linked to the number of cycles in the pulse. For high bandwidth cases, it is set at one cycle, for intermediate-bandwidth cases it is four cycles long and for the wavetrain case, twelve cycles are used in these calculations as an approximate representative of an infinite length signal. For instance, to achieve ω_{max} of 0.0528 (equivalent to 24 Hz) in a four-cycle pulse, we need $\omega_0 = 0.0533$. Since the signal is four cycles long, T_d is $4(2\pi/\omega_0) = 471.5$.

2.3. Joint study of the effects of frequency, bandwidth and amplitude

A factorial-type table of direct numerical simulation (DNS) runs was used to investigate the joint effects of frequency, bandwidth and amplitude of the wavepacket on the transition process. The full details of each initial wavepacket are given in Table 1. The cases are named according to the following convention. Each case is of the form _E-_F-_B where the letter E represents energy or power, F is frequency and B is bandwidth. The letters L, M and H denote low, medium and high respectively, and are filled into the blanks. So LE-MF-HB is a case with low energy, medium frequency and high (wide) bandwidth. As another example, consider LE-HF-LB, which represents low power, high frequency and low (narrow) bandwidth.

It might be worthwhile to explain the selection of amplitude for the initial disturbances. The amplitude is chosen to give rise to a fixed disturbance total energy or power. The distinction between power and energy needs to be made

Table 1. Parameters of the initial disturbance used to generate the wavepacket in each case.

Disturbance energy	Angular frequency, ω_{max}	Source driving frequency, ω_0	3-dB Bandwidth, $\Delta\omega$	Case name
1E	0.0259	0.0309	0.0292	LE-LF-HB
1E		0.0262	0.0058	LE-LF-MB
1P		0.0259	0.0019	LE-LF-LB
1E, 1P	0.0528	0.0630	0.0594	LE-MF-HB
1E		0.0533	0.0117	LE-MF-MB
1P		0.0528	0.0039	LE-MF-LB
1E	0.0776	0.0927	0.0874	LE-HF-HB
1E		0.0783	0.0172	LE-HF-MB
1P		0.0777	0.0057	LE-HF-LB
4E	0.0259	0.0309	0.0292	HE-LF-HB
4E		0.0262	0.0058	HE-LF-MB
4P		0.0259	0.0019	HE-LF-LB
4E	0.0528	0.0630	0.0594	HE-MF-HB
4E		0.0533	0.0117	HE-MF-MB
4P		0.0528	0.0039	HE-MF-LB
4E	0.0776	0.0927	0.0874	HE-HF-HB
4E		0.0783	0.0172	HE-HF-MB
4P		0.0777	0.0057	HE-HF-LB

because for the high and medium bandwidth cases, the parameter used is the total energy of the disturbance. On the other hand, for the low bandwidth wavetrains, they are continually excited by the source, so total disturbance energy would not be a constant and cannot be used as the characteristic parameter. Hence, for the wavetrains, the average power is used in place of the total disturbance energy. Furthermore, the energy is normalized with respect to the base case LE-MF-HB, and its energy and power are assigned units of 1E and 1P. Other disturbance energies are measured with respect to this base case. Therefore, the disturbance source in a case with 4P delivers four times the average power of the base case, and the initial disturbance in a case with 4E has four times the total energy of the base case.

For the angular frequency, the medium frequency, MF cases correspond to branch I (the lower-frequency branch) of the neutral stability curve at the disturbance source. The high frequency HF case is the mode with a high spatial growth rate, α_i (most linearly unstable) and the low frequency LF is in the linearly damped region.

2.4. Spectral analysis

Two-dimensional data of the velocity field is obtained by sampling along a spanwise line of fixed height. This produces data that varies in time and in the z-direction, and a Fourier transform of this data produces a power spectral density diagram, which displays spectral density as a function of frequency and spanwise wavenumber. Such spectral evolution sequences have been reported previously,[17] and for the large number of cases analysed in this study, listing a sequence of FFT plots for each case would result in far too many images. A sequence of velocity and spectral plots corresponding to the cases LE-MF-HB, -MB and LB has been published,[16] where they are known as the cycle, 4-cycle and wavetrain cases respectively.

Hence, a different way of summarizing and condensing the key information was found. This relies on the observation that the most active waves in the packet can be grouped into two categories two-dimensional and three-dimensional. Among the 3-D modes, the most significant is the subharmonic mode, because its dominance (or lack thereof) will determine whether the flow transitions to turbulence via the subharmonic N-regime, or takes the Klebanoff mode K-route. In the flow conditions of this DNS simulation, the subharmonic modes consistently had a spanwise wavenumber, β of about 0.125. So, it is possible to capture the key aspects of the wavepacket spatial development by focusing on the evolution of the modes with β equals to 0 (fundamental mode) and 0.125 (oblique subharmonic mode). Graphically, it can be displayed as a contour plot of mode amplitude as a function of angular frequency and Reynolds number.

2.5. Linear stability theory computations

Linear stability theory enables the prediction of the spatial growth of a mode with a given frequency and wavenumber. Curves of total amplification are readily available in the literature.[18] These curves usually show the linear growth factor $\ln(A/A_0)$. This enables us to determine the amplitude A at any spatial location, given the amplitude at one reference location A_0.

For comparison with the DNS simulations, the reference amplitude is the amplitude of the mode in the simulation at the first sampling point, located at $\mathrm{Re}_\delta = 1360$. In other words, the amplitudes of the modes in the DNS and LST plots are matched at the first point, and then the modes are allowed to evolve freely moving downstream. This first sampling point is located some distance downstream of the source (which is at $\mathrm{Re}_\delta = 1034$) to give time for the nonlinear transients associated with the disturbance generation process to decay.

Because wavepackets consist of a large number of modes, individual LST growth curves are unable to accurately capture the evolution of the system. In this work, an existing shooting-method LST code that computes the spatial amplification curve for one frequency-wavenumber mode at a time was available. This code was used as the core engine of a new program that computes the LST development of an ensemble of modes automatically. This program enabled the LST images in the results section to be quickly produced.

3. Results and Discussion

3.1. Transition types

The transition type of each case can be summarized in Table 2. It is found that bandwidth has the greatest effect on the transition process when the wavepacket has medium frequency, which is the frequency of branch I of the neutral curve at the disturbance source location.

Table 2. Summary of the transition type for each case. K denotes K-type transition with streaky structures (Klebanoff modes), while N denotes subharmonic transition. Cases marked as K→N represent a wavepacket that formed K-modes first, but they were later overshadowed in amplitude by the subharmonic mode, leading to final breakdown via a triad resonance and N-type transition. The superscript T indicates the transition type is for the transient front of the wavetrain only, while superscript R means that the main body of the wavetrain breaks down in the indicated manner. The * symbol indicates no breakdown to turbulence within the domain.

LOW ENERGY	**3dB Bandwidth ($\Delta\omega$)**		
Angular Frequency (ω)	Narrow	Intermediate	Wide
Low	K→N	N*	N
Medium	K	K→N	N
High	K→N^T	N*	N*

HIGH ENERGY	**3dB Bandwidth ($\Delta\omega$)**		
Angular Frequency (ω)	Narrow	Intermediate	Wide
Low	K	N	N
Medium	K	K	N
High	N^TK^R	N	N

One notable observation is that some wavetrains (narrow bandwidth disturbances) show different transition behaviour in their front and rear portions. Specifically, in the LE-HF-LB case, only the frontrunner (front portion of the wavetrain) breaks down to turbulence within the domain. This is similar to work by Sengupta on spatiotemporally growing wave fronts in spatially stable boundary layers.[20] Even though the boundary layer in our case is not spatially stable, there is still a significant difference in the growth rate of the wave front compared to the rest of the wavepacket. Sengupta concludes that the frontrunner is created by interactions between multiple stable modes. In our case we also believe that the frontrunner is created by interaction between components of the fundamental band. Due to edge effects, the frequency bandwidth of the front portion of the wavetrain is large, thus seeding a subharmonic mode that gives rise to N-type transition of the wavefront.

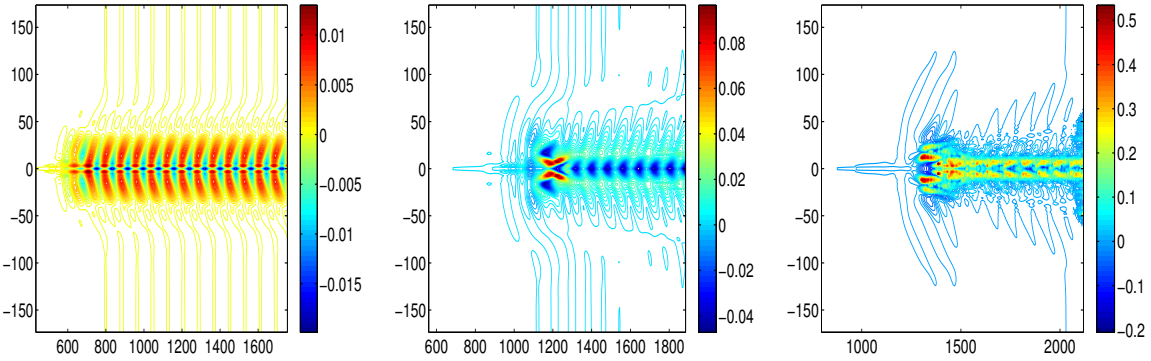

Fig. 1. HE-HF-LB u-velocity sampled at three different locations, left: $X = 604$, middle: $X = 776$, right: $X = 863$. Axes are T horizontal and Z vertical. The wavefront and the rest of the wavetrain show distinctly different transition behaviour. A horseshoe vortex forms at the wavefront, with a train of aligned λ vortices following behind.

Another interesting case is HE-HF-LB, in which both the frontrunner and the rest of the wavetrain breakdown to turbulence, but the front experiences N-type transition, while the rest undergoes K-type. Three snapshots of this transition process are shown in Fig. 1.

3.2. Spatial evolution of spectra

The figures 2, 3, 4 and 5 show the spatial evolution of 2D modes with zero spanwise wavenumber ($\beta = 0$) and oblique modes with the spanwise wavenumber of the subharmonic ($\beta = 0.125$). The plots are shaded with the mode amplitude according to the legend shown. All these diagrams show a general pattern. Far upstream, the flow is dominated by a 2D mode with the angular frequency of the disturbance source. This is the primary mode that is intended to be introduced into the flow. Nevertheless, because we are considering a wavepacket, this primary mode is accompanied by an ensemble of other modes.

As the wavepacket progresses downstream, all its component modes follow their respective LST spatial amplification curves for some distance, until a sufficiently high amplitude is reached for nonlinear effects to become significant. If the wavepacket bandwidth is wide, such as in Fig. 2, transition occurs through the subharmonic route. The signature for the appearance of the subharmonic mode is a large amplitude mode with $\beta = 0.125$ and a frequency of half the fundamental band. LST does not predict its growth correctly, because it is the result of difference interactions between component modes of the fundamental.[11] Once the subharmonic-fundamental wave triad is established, it grows rapidly due to a resonance mechanism. Finally, a rapid cascade of nonlinear interactions causes modes over a wide range of frequencies to suddenly proliferate, and such a broadening of the spectrum is an indication of incipient turbulence. Contrastingly, if the wavepacket bandwidth is narrow, intermediate stages of transition are not dominated by a subharmonic mode, but by very low-frequency Klebanoff modes or streaks causing K-type transition as in Fig. 3.

Another important indicator is the concentration of energy in the zero frequency, zero wavenumber mode, which points to a distortion of the mean flow profile, that is transitioning from the Blasius base flow to a turbulent boundary layer velocity profile.

It was also found that the flow has a preferred frequency, corresponding to branch I of the neutral stability curve at the disturbance source, given by $\omega_{pref} = 0.0528$ at $\mathrm{Re}_\delta = 1036$. If the wavepacket is initiated with a frequency different from ω_{pref}, the wavepacket frequency tends to shift to approach ω_{pref}. Such behaviour is evident in the medium frequency case LE-MF-HB in Fig. 2, and even more so when the initial frequency is higher, such as Fig. 4, where the change is dominant 2D frequency is dramatic and involves a discontinuous jump from $\omega \approx 0.07$ to $\omega \approx 0.05$ at $\mathrm{Re}_\delta \approx 1800$. Such behaviour is also well-predicted by LST, and can be attributed to the fact that the mode which starts at branch I of the neutral curve can continue to grow for the longest spatial distance, even as neighbouring modes start to go past their growth peaks and travel into slower growth or linearly damped Reynolds number regimes.

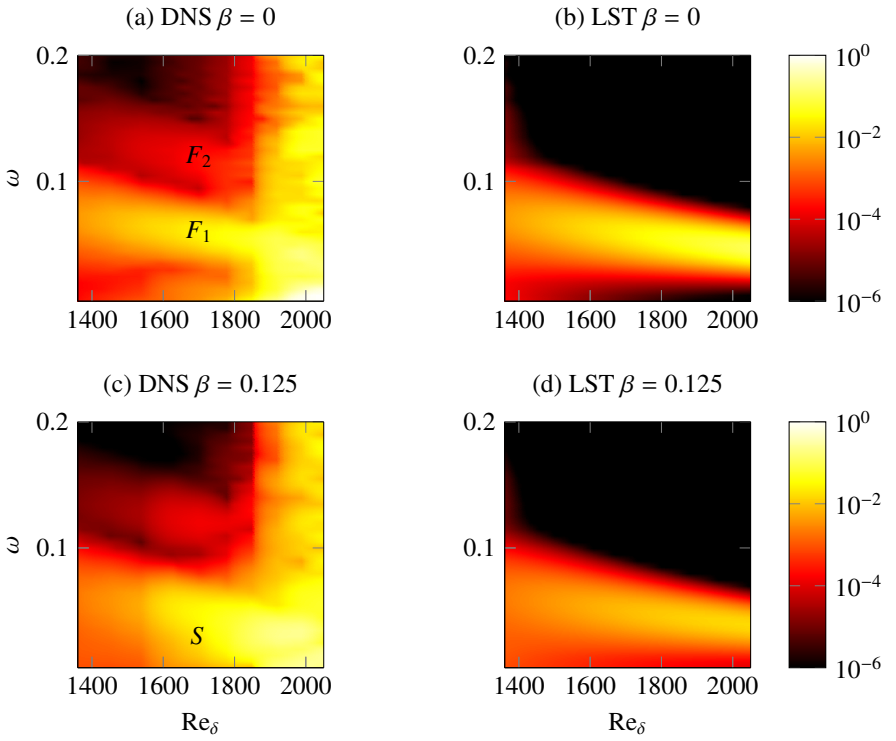

Fig. 2. The spatial evolution of 2D and 3D modes in the case LE-MF-HB. The fundamental mode and its harmonic are marked by F_1 and F_2 respectively in (a), and the subharmonic mode is labelled as S in (c). The behaviour of the 2D mode in the top row is well-predicted by LST, including the shift of the dominant frequency to lower values as the waves move downstream. The production of the subharmonic mode in the bottom row is a nonlinear phenomenon that is not predicted by LST. Transition occurs via the N-regime.

In addition, there is also some evidence of the dominant subharmonic frequency changing to track the corresponding change in dominant fundamental frequency. Such an observation can be made by looking at the DNS modes with $\beta = 0.125$ in Fig. 4(c).

Nevertheless, if the initial amplitude of the disturbance is increased, this will overwhelm the tendency for the flow to drift towards the preferred frequency, and the fundamental wave in the resonant triad responsible for breakdown to turbulence is at a higher frequency, corresponding to the initial wavepacket frequency. Such an inference can be derived from comparing the LE-HF-MB case with its higher-initial-energy counterpart, HE-HF-MB in Fig. 5. Another way of looking at this would be to say that the higher-frequency mode grows more slowly than the preferred mode, and would need a significant head start (in the form of higher initial amplitude) in order to win the race to turbulence.

Moreover, the higher initial energy also encouraged the formation of streaky structures, seen in the fairly large band of almost zero frequency in the DNS plot of spatial evolution of the $\beta = 0.125$ mode in Fig. 5(c). This indicated that transition initially proceeded through the K-type route, but ultimately the subharmonic mode grew to overshadow the Klebanoff modes and cause final transition via the N-route.

In the low-frequency cases, the linear damping of the dominant frequencies of the wavepacket mean that the wavepacket has almost been depleted of its low-frequency components by the time it reaches the first sampling location for the spectral analysis. Transition may still occur, but it usually involves a resonance among residual higher-frequency components close to the preferred resonant triad.

3.3. Identifying the modes that interact to produce the subharmonic

Fig. 6 plots the power spectra of the LE-MF-HB wavepacket streamwise velocity at three streamwise locations. The use of the logarithmic scale allows features to come to light across many orders of magnitude. Specifically, a region

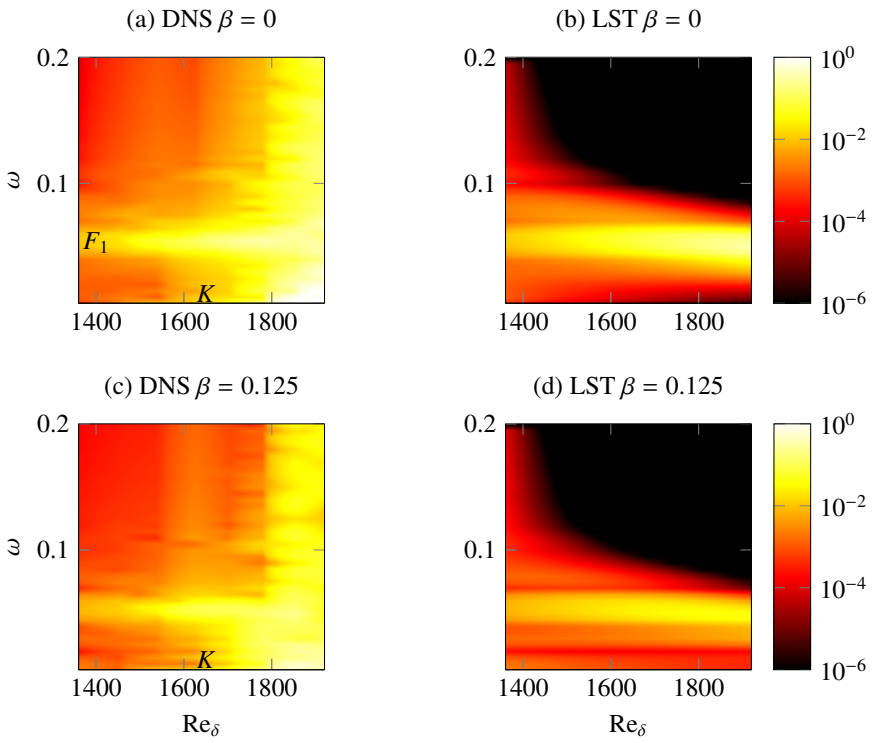

Fig. 3. Spatial evolution for the case LE-MF-LB. Transition proceeds through the K-route, and this is evident from the spectral broadening occurring almost in tandem for the fundamental and oblique modes. The signature streaky structures of Klebanoff modes, labelled K in (a) and (c), are also apparent as an almost zero-frequency band starting around $\mathrm{Re}_\delta = 1500$ in the oblique wave plot. The subharmonic mode never dominates the flow.

of interest is the higher harmonic of the fundamental. For example, at X=863, we have observed that the nonlinear interaction between mode 1 and mode 2 could give rise to mode 3. If the frequency and spanwise wavenumber of each mode is written as an ordered pair (ω, β),

$$(\beta_1, \omega_1) + (\beta_2, \omega_2) = (0.117, 0.064) + (0.117, 0.050) = (0.234, 0.114) \approx (\beta_3, \omega_3) \tag{1}$$

This lends further support to a fundamental thesis of Craik's paper,[11] that the components of the initial wavepacket are nonlinearly interacting with one another to produce the "seed" of the subharmonic. These interactions do not only cause the subharmonic to form, but spawn a host of other modes as can be seen in Fig. 6. The crux idea is to broaden our considerations beyond the first-order to consider the wider system of second-order modes created by quadratic interactions. Doing so enables a fuller and more complete picture of wavepacket evolution to come into focus.

4. Conclusion

A total of 18 different DNS and LST simulations were carried out with different combinations of initial wavepacket energy, frequency and frequency bandwidth. The key points are as follows. Wide bandwidth wavepackets generally undergo N-type transition. As the frequency bandwidth of the wavepacket is reduced, there is increased tendency towards K-type transition. The early development of narrow bandwidth wavepackets tends to be dominated by K-type processes; although their final breakdown may yet proceed via the N route for wavepackets with small initial amplitude (low energy). An increase in the energy level promotes K-type transition, especially for narrow bandwidth wavepackets.

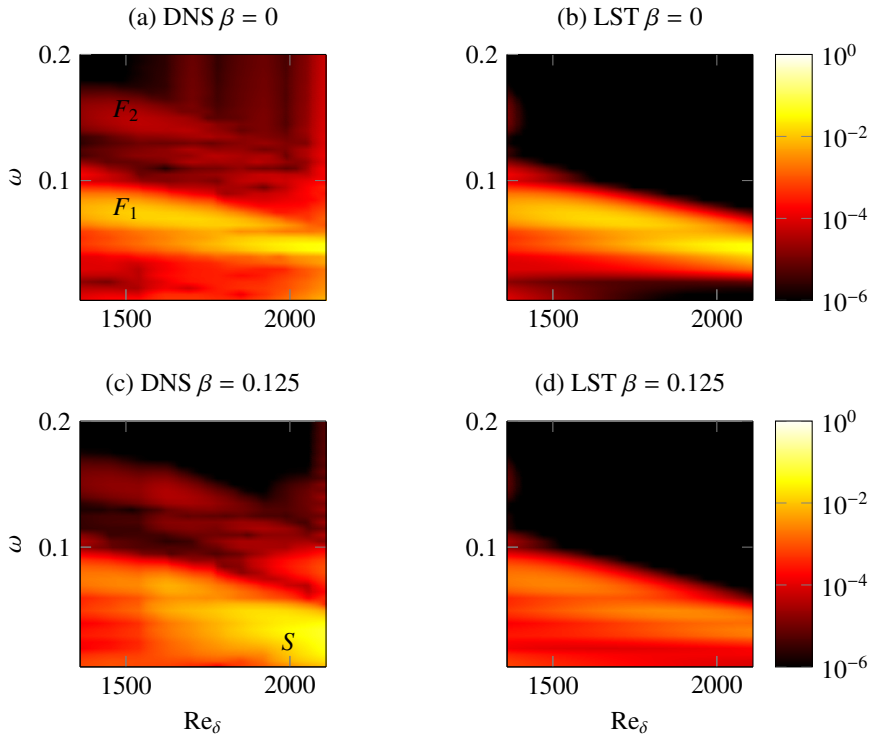

Fig. 4. Development of case LE-HF-MB. The initial fundamental and its harmonic are labelled F_1 and F_2 in (a). A discontinuous drop in the dominant 2D frequency is observable at Re_δ of around 1800. This brings the wavepacket frequency close to the preferred frequency. After the dominant 2D frequency shifts to $\omega \approx 0.05$, the subharmonic $\omega \approx 0.025$, marked S in (c) begins to grow strongly and leads the wavepacket into N-regime transition. By the end of the domain, the amplitude of the modes has increased by at least an order of magnitude, but the flow has not yet clearly transitioned to turbulence.

References

1. Boiko, A.V., Dovgal, A.V., Grek, G.R., Kozlov, V.V.. *Physics of Transitional Shear Flows*. Fluid Mechanics and Its Applications. Springer; 2012, .
2. Klebanoff, P.S., Tidstrom, K.D., Sargent, L.M.. The three-dimensional nature of boundary-layer instability. *J Fluid Mech* 1962;**12**(01):1–34.
3. Kachanov, Y.S.. Physical mechanisms of laminar-boundary-layer transition. *Annu Rev Fluid Mech* 1994;**26**(1):411–482.
4. Herbert, T.. Secondary instability of boundary layers. *Annu Rev Fluid Mech* 1988;**20**(1):487–526.
5. Craik, A.D.D.. Non-linear resonant instability in boundary layers. *J Fluid Mech* 1971;**50**(02):393–413.
6. Sayadi, T., Hamman, C.W., Moin, P.. Direct numerical simulation of complete H-type and K-type transitions with implications for the dynamics of turbulent boundary layers. *J Fluid Mech* 2013;**724**:480–509.
7. Breuer, K.S., Cohen, J., Haritonidis, J.H.. The late stages of transition induced by a low-amplitude wavepacket in a laminar boundary layer. *J Fluid Mech* 1997;**340**:395–411.
8. Cohen, J.. The initial evolution of a wave packet in a laminar boundary layer. *Phys Fluids* 1994;**6**(3):1133–1143.
9. Cohen, J., Breuer, K.S., Haritonidis, J.H.. On the evolution of a wave packet in a laminar boundary layer. *J Fluid Mech* 1991;**225**:575–606.
10. Stein, E.M., Shakarchi, R.. *Fourier Analysis: An Introduction*. Princeton University Press; 2003.
11. Craik, A.D.D.. A model for subharmonic resonance within wavepackets in unstable boundary layers. *J Fluid Mech* 2001;**432**:409–418.
12. Medeiros, M.A.F., Gaster, M.. The influence of phase on the nonlinear evolution of wavepackets in boundary layers. *J Fluid Mech* 1999; **397**:259–283.
13. Medeiros, M.A.F., Gaster, M.. The production of subharmonic waves in the nonlinear evolution of wavepackets in boundary layers. *J Fluid Mech* 1999;**399**:301–318.
14. Medeiros, M.A.F.. Nonlinear wavepackets in boundary layers. In: Govindarajan, R., editor. *Sixth IUTAM Symposium on Laminar-Turbulent Transition*; vol. 78 of *Fluid Mechanics and Its Applications*. Springer Netherlands; 2006, p. 317–322.
15. de Paula, I.B., Würz, W., Krämer, E., Borodulin, V.I., Kachanov, Y.S.. Weakly nonlinear stages of boundary-layer transition initiated by modulated Tollmien-Schlichting waves. *J Fluid Mech* 2013;**732**:571–615.
16. Kang, K.L., Yeo, K.S.. The effect of wavepacket frequency bandwidth on the laminar-turbulent transition process in a Blasius boundary layer. *AIAA Paper 2013-2615* 2013;.

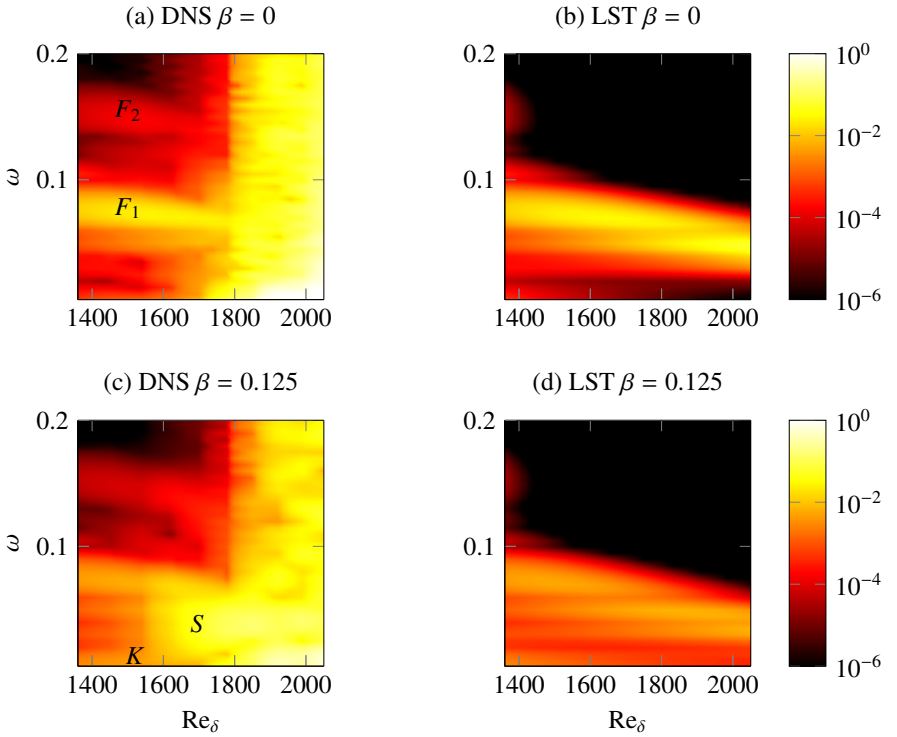

Fig. 5. The case HE-HF-MB. The higher initial energy and amplitude of the mode sets it apart from LE-HF-MB in Fig. 4. It now no longer follows the LST predictions of drift to lower frequencies. Instead, the 2D fundamental remains close to its initial frequency, K-modes form initially, but then the subharmonic forms at approximately half the fundamental frequency, leading to rapid N-type transition to turbulence.

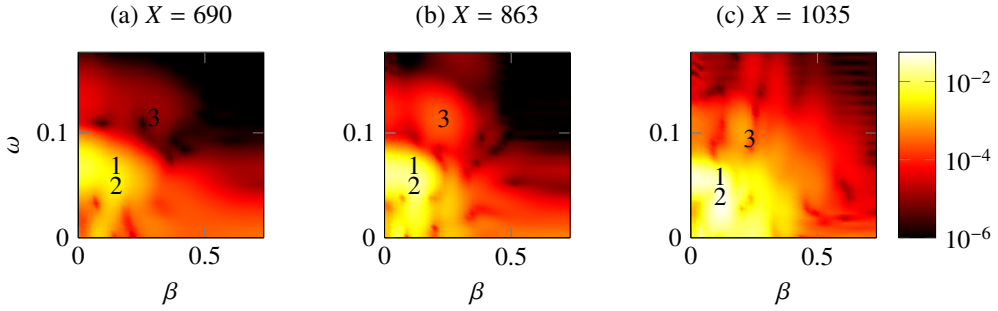

Fig. 6. Power spectra of the LE-MF-HB perturbation u-velocity at various streamwise locations.

17. Yeo, K.S., Zhao, X., Wang, Z.Y., Ng, K.C.. DNS of wavepacket evolution in a Blasius boundary layer. *J Fluid Mech* 2010;**652**:333–372.
18. Jordinson, R.. The flat plate boundary layer. Part 1. Numerical integration of the Orr-Sommerfeld equation. *J Fluid Mech* 1970;**43**(04):801–811.
19. Wang, Z.Y., Yeo, K.S., Khoo, B.C.. Spatial direct numerical simulation of transitional boundary layer over compliant surfaces. *Comput Fluids* 2005;**34**(9):1062–1095.
20. Sengupta, T.K., Rao, A.K., Venkatasubbaiah, K.. Spatiotemporal growing wave fronts in spatially stable boundary layers. *Phys Rev Lett* 2006;**96**(22):224504.